Global gyrokinetic simulations of ion temperature gradient-driven instabilities in optimised stellarators

M. D. J. Cole[1], R. Hager[1], T. Moritaka[2], S. Lazerson[1], S. Ku[1], C. S. Chang[1]

[1] *PPPL, Princeton, USA*

[2] *NIFS, Toki, Japan*

Introduction

Developments in stellarator optimisation have led to designs where transport is expected to dominated by turbulent rather than neoclassical transport. This has been observed in the recent Wendelstein 7-X (W7-X) OP 1.2 experimental campaign [1]. This calls for improved numerical tools to enable simulation of turbulent transport in stellarators with comparable fidelity to those performed for tokamaks. So far, reduced delta-f gyrokinetic simulations have been published using a linear model global to the last closed flux surface with the EUTERPE code [7], and using a nonlinear flux tube ensemble model to the last closed flux surface with the GENE code [8].

In recent work, the XGC full volume gyrokinetic code has been extended for stellarator geometry (XGC-S) [3]. It has been verified for reduced delta-f linear gyrokinetics global to the last closed flux surface in Wendelstein 7-X geometry [2, 4]. In on-going work, the code is being applied to a range of optimisation concepts, including the proposed quasiaxisymmetric device QUASAR. The code is also being extended to full volume equilibria including islands and stochastic fields, and to nonlinear simulations.

In this work, we report on these developments.

Quasiaxsymmetric and quasiisodynamic stellarators

Simulations have been performed in Wendelstein 7-X and QUASAR geometry. This tests the ability of the XGC-S code to deal with differing highly shaped stellarator geometries. It also allows some comparison between the properties of the two devices. Simulations are performed with a temperature gradient localised at normalised poloidal flux $s = 0.5$. Here, $a/L_T = 3.0$, for

$$\frac{\mathrm{d}\ln T}{\mathrm{d}\, s} = -\sqrt{2}\left(\frac{1}{2} - |\, s - \frac{1}{2}\,|\right)\frac{a}{L_T}, \tag{1}$$

where T is the ion temperature, s is the normalised flux, a is the minor radius (here, 0.505 m) and L_T is the temperature gradient scale length. A flat density profile has been used.

The calculated linear growth rate is $\gamma_{QUASAR} = 0.151 c_s/a$, with corresponding $\gamma_{W7-X} = 0.11 c_s/a$. c_s is the normalised thermal velocity in the plasma. Corresponding flux tube calculations published recently for QUASAR found a higher growth rate of $\gamma_{QUASAR} > 0.3 c_s/a$ [5].

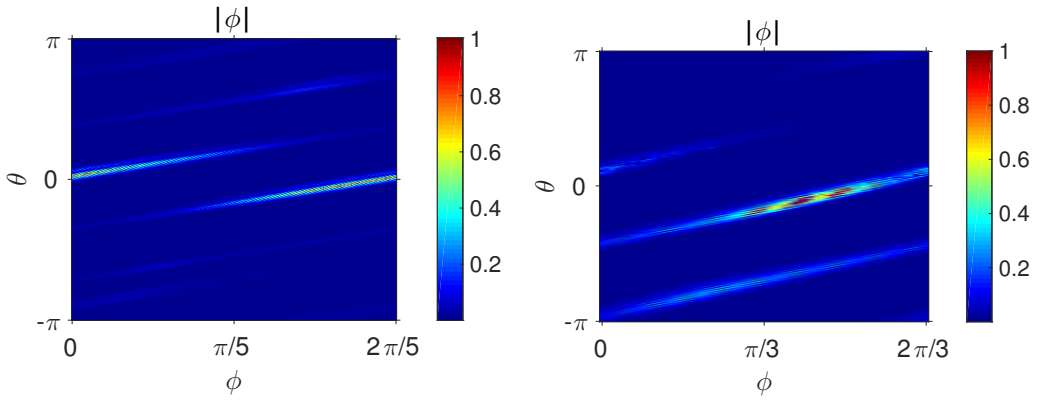

Figure 1: *Linear ITG mode structure in Wendelstein 7-X (left) and QUASAR (right).*

This is consistent with previous numerical observations that flux surface growth rates in stellarators can be lower than those of the fastest growing flux tube [8]. In Figure. 1 the electrostatic potential structure is compared in the two devices in toroidal and poloidal angle. Both devices exhibit strong localisation in poloidal angle and weaker localisation in toroidal angle.

Nonlinear benchmarking

Prediction of turbulent transport requires nonlinear simulations. Despite some useful efforts, saturated nonlinear heat fluxes cannot be reliably predicted in general by linear growth rates. The XGC-S code is being developed to enable nonlinear simulations. As a first step, a CYCLONE-like tokamak case is calculated with both the conventional XGC1 code and the new XGC-S code. This case has been benchmarked extensively with XGC1 against other global gyrokinetic tokamak codes, such as ORB5 and GENE. For linear simulations, the benchmark has already been successfully performed comparing XGC1 and XGC-S [4].

In Figure. 2, we plot the evolution of the average electrostatic potential in the linear and nonlinear phases as calculated with XGC1 and XGC-S. A close agreement in seen in both cases. Note that the exact behaviour in the saturated nonlinear phase is different in general, as the course of the potential evolution is very sensitive to the initial conditions. The XGC1 and XGC-S codes differ in the tokamak case principally in terms of the mesh setup and the equilibrium calculation and interpolation [3, 4].

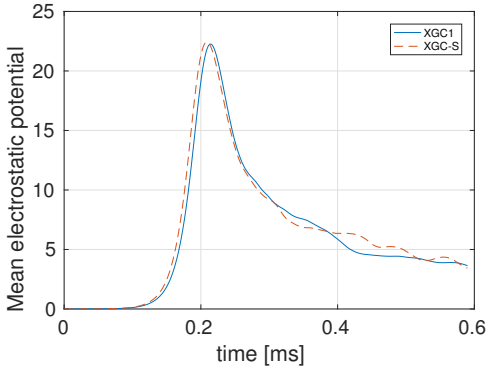

Figure 2: *Comparison of the nonlinear evolution of the average electrostatic potential for conventional XGC1 and XGC-S.*

As a further test of the correctness of the XGC-S implementation for nonlinear simulations, we com-

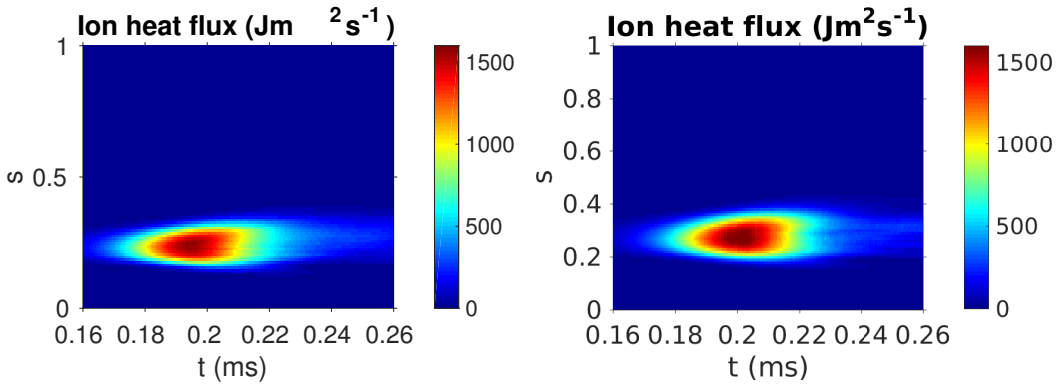

Figure 3: *Ion heat flux calculated by XGC1 (left) and XGC-S (right) in a circular tokamak-like case.*

pare the ion heat flux at the peak of saturation of the mode. In Figure. 3, the radial and time dependence of the heat flux is plotted for the two codes. Note that each simulation was initialised with the same starting perturbation and run for the same length of time before reaching this point. Close agreement is seen in the calculated values.

It should be noted that a small shift in the radial location is due to slightly different definitions of s used in the two codes.

Extended equilibria

It is important to simulate realistic stellarator fields to the first wall in the long term outlook of XGC-S. So far, XGC-S, like most stellarator gyrokinetic codes, has taken its equilibrium data from the VMEC code. The VMEC code assumes nested flux surfaces. In recent work, an interface for the HINT3D code has been developed for XGC-S. The HINT3D code permits resistive relaxation and therefore stochastic fields and magnetic islands to develop [6].

In Figure. 4, we compare core stochastic losses of energetic particles through the last closed flux surface in the Wendelstein 7-X stellarator for equilibria calculated with the VMEC and HINT3D codes. In Wendelstein 7-X, the largest islands are in the edge region, so the difference in loss rate is expected to be slight, as is observed in these first simulations. This benchmark demonstrates the ability of XGC-S to use general HINT3D equilibria, a capability that will be matched with existing capability to model the first wall [3].

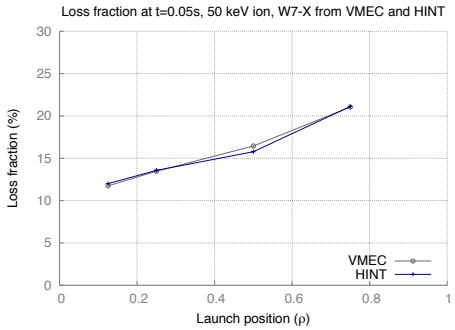

Figure 4: *Comparison of stochastic particle losses in the core region of W7-X with VMEC and HINT3D equilibria.*

In Wendelstein 7-X, the behaviour of islands is

particularly important for divertor operation. In future edge physics simulations, correct modelling of this physics will be vital.

Conclusion

In this work, we show that the XGC-S code has established capabilities in simulating a range of stellarator physics. It can be applied to multiple optimisation concepts, to nonlinear simulations (currently only verified in tokamaks) and to extended equilibria which relax the assumption of nested flux surfaces. Initial results demonstrate that linear ITG modes, quasi-localised by the application of a narrow temperature gradient, exhibit strong poloidal and toroidal localisation in both the quasi-isodynamic Wendelstein 7-X stellarator and the quasi-axisymmetric QUASAR stellarator proposal. With the same normalised temperature gradient applied at the same radial location in normalised poloidal flux, the linear growth rate in QUASAR is somewhat higher than in Wendelstein 7-X. In QUASAR, we observe the same tendency previously found in simulations of Wendelstein 7-X for surface or fully global linear growth rates to generally be lower than those of individual fast growing flux tubes.

In future work, the nonlinear capability of XGC-S will be fully benchmarked in the circular tokamak case, and then applied to QUASAR and Wendelstein 7-X geometry. The effects of a radially global as opposed to flux tube or flux tube ensemble model will be investigated, including the effects of global profiles in temperature and density. The model will be extended to total-f including general equilibria to the first wall. The effects of collisions will be considered, using the nonlinear collision operator currently implemented in XGC1. The ultimate goal of this work is to apply high performance computing to understand present stellarator experiments and to contribute to future designs with, for instance, improved optimisation to minimise turbulent transport.

References

[1] T. Klinger *et al.*, Nucl. Fusion **59** 112004 (2019)

[2] M. D. J. Cole *et al.*, Phys. Plasmas **26** 032506 (2019)

[3] T. Moritaka *et al.*, Plasma **2** (2), 179-200 (2019)

[4] M. D. J. Cole *et al.*, Phys. Plasmas, accepted (July 2019)

[5] S. Lazerson *et al.*, Phys. Plasmas **26** 022509 (2019)

[6] Y. Suzuki *et al.*, Plasma Phys. Control. Fusion **59** 054008 (2017)

[7] J. Riemann *et al.* Plasma Phys. Control. Fusion **58** 074001 (2016)

[8] P. Xanthopoulos *et al.* Phys. Rev. Lett. **113** 155001 (2014)